Nonequilibrium excitations in ferromagnetic nanoparticles

Silvia Kleff[1,2,*] and Jan von Delft[1]
[1]*Center for NanoScience and Sektion Physik, Ludwig-Maximilians-Universität, Theresienstrasse 37, 80333 München, Germany*
[2]*Institut für Theoretische Festkörperphysik, Universität Karlsruhe, 76128 Karlsruhe, Germany*
(Received 17 October 2001; revised manuscript received 1 February 2002; published 3 June 2002)

In recent measurements of tunneling transport through individual ferromagnetic Co nanograins, Deshmukh, Guéron, Ralph *et al.* (DGR) [Phys. Rev. Lett. **83**, 4148 (1999); M. M. Deshmukh *et al.*, *ibid.* **87**, 226801 (2001)] observed a tunneling spectrum with discrete resonances, whose spacing was much smaller than what one would expect from naive independent-electron estimates. In a previous publication [S. Kleff, J. von Delft, M. Deshmukh, and D. C. Ralph, Phys. Rev. B **64**, 220401 (2001)], we had suggested that this was a consequence of nonequilibrium excitations, and had proposed a ''minimal model'' for ferromagnetism in nanograins with a discrete excitation spectrum as a framework for analyzing the experimental data. In the present paper, we provide a detailed analysis of the properties of this model: We delineate which many-body electron states must be considered when constructing the tunneling spectrum, discuss various nonequilibrium scenarios, and compare their results with the experimental data of DGR. We show that a combination of nonequilibrium spin and single-particle excitations can account for most of the observed features, in particular the abundance of resonances, the resonance spacing, and the absence of Zeeman splitting.

DOI: 10.1103/PhysRevB.65.214421 PACS number(s): 75.50.Cc, 73.23.Hk, 73.40.Gk

I. INTRODUCTION

An important milestone in the study of itinerant ferromagnetism was reached during the last two years, when Deshmukh, Guéron, Ralph *et al.*[1,2] (DGR), using single-electron tunneling spectroscopy,[4] succeeded for the first time in resolving discrete resonances in the tunneling spectrum through individual ferromagnetic single-domain cobalt nanograins, with diameters between 1 and 4 nm. Their work goes beyond previous studies of ferromagnetic single-electron transistors,[5–8] which elucidated the interplay of ferromagnetism and charging effects: the fact that DGR's Co grains were sufficiently small such that discrete resonances could be resolved means that they were probing the true quantum states participating in electron tunneling, which allows the nature of electron correlations in itinerant ferromagnets to be studied in unprecedented detail. Besides the intrinsic scientific interest in studying ferromagnetism on the nanometer scale, the insights so gained might also be of technological interest, since the size of memory elements in magnetic storage technologies is decreasing extremely rapidly,[9] and particles as small as 4 nm are coming under investigation.[10]

An examination of the magnetic-field dependence of the individual resonances observed by DGR indicated that two-current models, in which spin-up and spin-down electron bands are considered effectively independently, are inadequate for describing the true electronic states inside a nanometer-scale ferromagnet—so that a fundamentally different theoretical approach is required. To this end, a simple phenomenological model was recently introduced by the present authors together with Deshmukh and Ralph,[3] and independently by Canali and MacDonald.[11] We regard this as a ''minimal model'' for ferromagnetic nanograins, in that it seems to be the simplest model possible for a discrete-state system which takes into account the electronic correlations induced by magnetic interactions and which treats the particle's total spin as a quantum-mechanical variable. We argued[3] that the main features of the measured tunneling spectra can be understood within this model by assuming that nonequilibrium spin accumulation occurs, which can produce a much denser spectrum of tunneling excitations than expected within an independent-electron model. The conclusion that nonequilibrium effects play an important role has since been confirmed by more recent measurements by DGR (Ref. 2) on a gated device, in which new resonances appeared as the gate voltage was tuned to drive the system further away from equilibrium.

In the present paper, we provide a detailed analysis of equilibrium and nonequilibrium tunneling through ferromagnetic grains, within the framework of our minimal model. The present analysis goes well beyond that of Ref. 3, in that we consider not only the spin ground states of Fig. 2 in Ref. 3, but also spin-wave excitations and single-particle excitations. The latter turn out to be necessary to understand why a small resonance spacing is observed even when the threshold bias voltage for the onset of tunneling is rather small, so that nonequilibrium effects cannot be very strong.

The structure of the paper is as follows. In Sec. II we summarize the experimental results of Deshmukh *et al.*[2] and Guéron *et al.*[1] The Hamiltonian of our minimal model is presented in Sec. III, together with a convenient set of basis states for analyzing the low-lying excitations and their energies. In Sec. IV we discuss two different equilibrium excitations in ferromagnetic grains, namely, single-particle excitations and spin excitations. A detailed discussion of nonequilibrium excitations and their consequences for tunneling spectra is given in Sec. V: First we calculate the current through a grain for a nonequilibrium scenario involving only transitions between the ground states $|s,s\rangle$ of a ladder of spin multiplets of different total spin s; the resonance spacing for the peaks in the conductance is found to be in quantitative agreement with DGR's measurements if we assume a total ground-state spin of about $s_0 \simeq 1000$ and that the

resonances are predominantly due to the tunneling of minority electrons. We then generalize this nonequilibrium scenario by including also all more highly excited states $|s,m\rangle$ of these spin multiplets, finding that if the total spin is large ($s \gg 1$), the Zeeman splitting of the observed resonances should be strongly suppressed, in agreement with DGR's experiments. Finally, we show that a combination of single-particle and spin excitations in the presence of nonequilibrium can lead to the large number of resonances seen in experiments. Some concluding remarks can be found in Sec. VI.

A brief account of our results on the most simple nonequilibrium scenario in ferromagnetic grains has already been given in Ref. 3. The present paper includes a detailed derivation of these results (Sec. V B), since this paves the way for the more complicated nonequilibrium scenarios presented in Sec. V C and Sec. V D, which have not been reported before.

II. SUMMARY OF EXPERIMENTAL RESULTS

In DGR's experiments,[1,2] a nanoscale cobalt grain was used as a central island in a single-electron transistor: it was connected via tunnel barriers to external leads and for one of the grains in Ref. 2, the central grain was also capacitively coupled to a gate. The electronic spectrum of the particle was determined by measuring the tunnel conductance through the grain as a function of transport voltage (V) [gate voltage (V_g)] and magnetic field $\mu_0 H$ at a fixed temperature of $\lesssim 90$ mK. The diameters of the Co grains were estimated to be 1–4 nm. Assuming a roughly hemispherical shape, the number of atoms in each grain then was in the range $N_a \approx 20$–1500, implying a total spin of $s_0 \approx 0.83 N_a \approx 17$–$1250$.

Since the charging energy (>30 meV) was very much larger than typical values of the transport voltage ($eV < 9$ meV) and the temperature, fluctuations in electron number on the grain are strongly suppressed, so that coherent superposition between different electron numbers N need not be considered. The energy balance condition that determines through which eigenstates of the grain electrons can tunnel for given values of transport (and gate) voltage thus involve differences between eigenenergies of a grain with a *fixed particle number* N or $N \pm 1$,[12]

$$\Delta E_{fi}^{\pm} \equiv E_f^{N\pm 1} - E_i^N , \tag{1}$$

each corresponding to the energy cost of some rate-limiting electron-tunneling process $|i\rangle^N \rightarrow |f\rangle^{N\pm 1}$ onto or off the grain. Here $|i\rangle^N$ denotes a discrete eigenstate, with eigenenergy E_i^N, of a grain with N electrons, etc. As the magnetic field H is swept, the resonances undergo energy shifts and crossings.

The excitation spectra measured by DGR had several properties that differ strikingly from those of previously studied nonmagnetic Al and Au grains[4,13] including the following: (P1) Many *more low-energy excitations* were observed than expected: For all Co grains studied, the observed level spacing is $d_{\rm obs} \lesssim 0.2$ meV, which is much *smaller* than the independent-electron estimate of $d_{\rm min} \approx 1.2\ {\rm eV}/s_0$ and $d_{\rm maj} \approx 4.6\ {\rm eV}/s_0$ for minority/majority electrons,[14,15] respectively. (In Ref. 2 many more resonances were observed than in Ref. 1, due to lower-noise tunnel barriers.)

(P2) In the small-field regime ($\mu_0 H < 0.2$ T), the tunneling resonance energies show strong nonlinear dependence on H, with hysteresis and jumps at the switching field $|H_{\rm sw}|$. For fields beyond the switching field, the levels can exhibit nonmonotonic variations as a function of H, with each level behaving differently. For a more detailed discussion of the magnetic-field dependence of the tunneling energies see Refs. 2 and 3.

(P3) In the large-field regime ($|H| \gg |H_{\rm sw}|$), the resonances depend roughly linearly on H, with H slopes that almost all have the same sign for a given grain, i.e., slopes of opposite signs due to Zeeman shifting of spin-up and spin-down levels[4,13] are not observed.

(P4) Measurements on a gated device[2] showed that the observed resonances correspond predominantly to the tunneling of minority electrons.

(P5) Measurements on a gated device[2] also showed that *some* of the resonances must be due to nonequilibrium excitations, since some (but not all) resonances disappear when the Coulomb-blockade threshold for the onset of tunneling (i.e., the amount of nonequilibrium) is reduced by tuning the gate voltage to lie close to a degeneracy point.

We will argue below that the *main* features of the measured tunneling spectra, as summarized above, can be qualitatively understood within our model. However, we will not attempt to give an overly detailed *quantitative* comparison with experimental data for *every* aspect of the experiment. In view of the richness of DGR's experimental data, especially the very complicated magnetic-field dependence of resonances, such a goal would clearly be overambitious. Instead we shall strive to understand the main trends and features of the experiment, e.g., the absence of Zeeman splitting and the role played by nonequilibrium, and do a quantitative comparison only for a few selected quantities, e.g., the resonance spacing.

III. MODEL

In this section we introduce a simple model for ultrasmall ferromagnetic grains. The challenge is to describe the individual quantized electronic excitations of a ferromagnetic nanoparticle, taking into account the electronic correlations induced by magnetic interactions and anisotropy forces.

A. Hamiltonian

We propose to model a nanoscale magnet with discrete excitations by the following "minimal" Hamiltonian:[3,16]

$$\mathcal{H} = \mathcal{H}_C + \mathcal{H}_0 + \mathcal{H}_{\rm exch} + \mathcal{H}_{\rm Zee} + \mathcal{H}_{\rm uni} , \tag{2a}$$

$$\mathcal{H}_C = eV_D \delta\hat{N} + E_C \delta\hat{N}^2 , \tag{2b}$$

$$\mathcal{H}_0 = \sum_{j\sigma} \varepsilon_j c_{j\sigma}^{\dagger} c_{j\sigma} , \tag{2c}$$

$$\mathcal{H}_{\rm exch} = -\frac{U}{2}\vec{S}\cdot\vec{S}, \tag{2d}$$

$$\mathcal{H}_{\rm Zee} = -hS^z, \tag{2e}$$

$$\mathcal{H}_{\rm uni} = -k_N(\vec{S}\cdot\hat{n})^2/s_0, \tag{2f}$$

with $h = g_{\rm eff}\mu_B\mu_0 H$. Here $\mathcal{H}_C$ is the standard Coulomb charging energy for a nanoparticle with δN excess electrons. $V_D = [Q_0 + \Sigma_r V_r C_r]/C$, for $r = (L,R,g)$, is the electrostatic potential energy of the island, with $C \equiv \Sigma_r C_r$. C_L, C_R, and C_g are the tunnel junctions connecting the grain to the left or right lead or the gate electrode, respectively, and V_L, V_R, and V_g are the voltages of the left/right leads and the gate electrode. Q_0 is an initial random offset charge and $E_C = e^2/2C$ is the unit of charging energy.

$\mathcal{H}_0$ describes the kinetic energy of a single band of single-electron states $|j,\sigma\rangle$, labeled by a discrete index j and a spin index $\sigma = (\uparrow,\downarrow)$, with the spin-quantization axis chosen in the z direction. The exchange, Zeeman, and anisotropy terms, $\mathcal{H}_{\rm exch}$, $\mathcal{H}_{\rm Zee}$, and $\mathcal{H}_{\rm uni}$, are functions of the total spin vector $\vec{S} = \Sigma_j \vec{S}_j$, where $\vec{S}_j$ is the spin vector of the electrons in level j,

$$\vec{S}_j = \frac{1}{2}\sum_{\sigma'\sigma} c^\dagger_{j\sigma}\vec{\sigma}_{\sigma\sigma'}c_{j\sigma'} \tag{3}$$

($\vec{\sigma}$ are Pauli matrices). $\mathcal{H}_{\rm exch}$ is a rotationally invariant term which models the effects of an exchange field and forces the system to adopt a nonzero total ground-state spin, say, s_0. On account of this term, spins aligned parallel or antiparallel to $\langle\vec{S}\rangle$ may be thought of as forming ''majority'' and ''minority'' bands, which effectively rotate rigidly together with the magnetization direction. We shall take the mean level spacings near the respective Fermi energies, $d_{\rm min} \approx 1.19\ {\rm eV}/s_0$ and $d_{\rm maj} \approx 4.61\ {\rm eV}/s_0$, and the exchange splitting of the Fermi energies, $\Delta_F \equiv \varepsilon_{F,\rm maj} - \varepsilon_{F,\rm min}$ (≈ 2 eV for Co),[14] as characteristic parameters of the model.

$\mathcal{H}_{\rm Zee}$ describes the spin Zeeman energy in an external magnetic field $\vec{H} = H\hat{z}$. Finally, the uniaxial anisotropy $\mathcal{H}_{\rm uni}$ is the simplest nontrivial form of an anisotropy modeling the combined effects of crystalline, shape, and surface anisotropies, etc.[17] $\hat{n}$ is the unit vector in the easy-axis direction and $k_N(>0)$ is a volume-independent constant. k_N can be estimated from the measured switching field using $k_N \approx \mu_0\mu_B H_{\rm sw}$, which yields $k_N \approx 0.01$ meV (see Ref. 14 of Ref. 3). For completeness we note that our analysis in a previous paper (Ref. 3, see also Ref. 2) showed that the anisotropy constant k_N undergoes fluctuations, i.e., varies between different electronic states within a ferromagnetic nanoparticle. It was shown that these fluctuations have significant consequences for the magnetic-field dependence of the resonance energies. However, in the present paper we shall focus only on understanding the characteristic spacings between resonances observed in DGR's experiments, and not on their magnetic-field dependence; we will therefore neglect fluctuations in k_N throughout this paper.

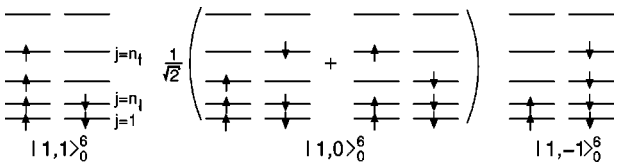

FIG. 1. The spin-wave multiplet $|s,m\rangle_0^N$ for $s=1$, $N=6$. The position of each level represents its kinetic energy ε_j.

B. Basis states

Let us for the moment set the anisotropy strength $k_N = 0$, and use the eigenstates of $\mathcal{H}(k_N=0)$ to construct a convenient set of ''bare'' basis states. Since the Hamiltonian then commutes with the total spin, these states can be grouped into spin multiplets that are labeled by their $\vec{S}\cdot\vec{S}$ and S^z eigenvalues, say, $s(s+1)$ and m. For example, the bare ground state of $\mathcal{H}(k_N=0)$ for given N, s, and $h(>0)$, say, $|s,s\rangle_0^N$, can be written explicitly as a member of the following multiplet of normalized states, $|s,m\rangle_0^N$ (illustrated in Fig. 1):

$$|s,s\rangle_0^N \equiv \prod_{j=1}^{n_\uparrow} c^\dagger_{j\uparrow}\prod_{j=1}^{n_\downarrow} c^\dagger_{j\downarrow}|{\rm vac}\rangle, \tag{4}$$

$$|s,m\rangle_0^N \equiv \sqrt{\frac{(s+m)!}{(2s)!(s-m)!}}(S_-)^{(s-m)}|s,s\rangle_0^N. \tag{5}$$

Here $n_{\uparrow/\downarrow} = N/2 \pm s$, and $S_- = \Sigma_j c^\dagger_{j\downarrow}c_{j\uparrow}$ is the spin-lowering operator. Within this model, the energy difference between the spin multiplet $|s,m\rangle$ and all other states that are constructed from the same single-electron levels is at least of order $\varepsilon_{F,\rm maj} - \varepsilon_{F,\rm min}$, a very large value ($\simeq 2$ eV for Co).[14]

The inclusion of a nonzero anisotropy term, $\mathcal{H}_{\rm uni}$, will cause the true low-energy eigenstates, $|s,m\rangle^N$, to be linear superpositions of the bare states in the multiplet $|s,m\rangle_0^N$. We choose labels such that $|s,m\rangle^N \to |s,m\rangle_0^N$ as $k_N/h \to 0^+$. We shall call the states $|s,m\rangle^N$ the *spin-wave multiplet*, since each can be viewed as a homogeneous spin wave.

C. Eigenenergies

In the absence of anisotropies ($\mathcal{H}_{\rm uni}=0$), it is possible to write explicit expressions for the low-lying excitation energies of our model. Let us denote the excitation energy of a state $|s,m\rangle_0^N$ relative to the ground state $|s_0,m_0\rangle_0^{N_0}$ (for a gated device) by[12]

$$\delta E(\delta s, \delta m, \delta N) + eV_D\delta N, \tag{6}$$

with $\delta s = s - s_0$, $\delta m = m - m_0$, and $\delta N = N - N_0$. It is straightforward to show that the voltage-independent contribution to Eq. (6) has the following form, written by Canali and MacDonald:[11]

$$\delta E(\delta s,\delta m,\delta N) = (\delta N)^2\left[\frac{d_{\rm maj}}{8}+\frac{d_{\rm min}}{8}+E_C\right]+\delta N\left[\overline{\varepsilon}_F+\frac{d_{\rm maj}}{4}+\frac{d_{\rm min}}{4}\right] + \frac{(\delta s)^2}{2}[d_{\rm maj}+d_{\rm min}-U]+\delta s\left[\Delta_F-U(s_0+1/2) + \frac{d_{\rm maj}}{2}-\frac{d_{\rm min}}{2}\right]+\delta s\,\delta N\left[\frac{d_{\rm maj}}{2}-\frac{d_{\rm min}}{2}\right]-h\,\delta m. \quad (7)$$

Here we introduced the average of majority- and minority-band Fermi energies $\overline{\varepsilon}_F=(\varepsilon_{F,\rm maj}+\varepsilon_{F,\rm min})/2$. The stability of the ground-state spin s_0, i.e., the requirement that $\delta E(\delta s,\delta m,\delta N)>0$, implies[11] the relation $\Delta_F=U(s_0+1/2)+d_0$, where $d_0(\sim 1/s_0)$ is a small, grain-dependent energy satisfying

$$-(d_{\rm maj}-U/2)+h<d_0<d_{\rm min}-U/2+h. \quad (8)$$

Hence, the magnitude of U may be estimated as $U\simeq\Delta_F/s_0\simeq 2$ eV$/s_0$. Note that the ground-state spin s_0 can be changed by a sufficiently large change in applied magnetic field. However, the range over which the applied magnetic field has to be swept between two successive changes in ground-state spin is of order $\delta h\simeq(d_{\rm maj}+d_{\rm min}-U)/2$, which is large in nanomagnets ($\mu_0\delta H\gtrsim 25$ T for Co particles with diameters $\lesssim 4$ nm). Therefore, for a given value of N, we shall, as long as we neglect nonequilibrium effects, consider only the "ground-state" spin value s_0.

IV. EQUILIBRIUM TRANSITIONS

To construct the tunneling spectrum associated with, say, adding an electron to the grain, we must, in principle, calculate the excitation energies ΔE^+_{fi} for all the allowed transitions, i.e., those for which the tunneling matrix element

$$M^{j\sigma}_{fi}\equiv {}^{N+1}\langle f|c^\dagger_{j\sigma}|i\rangle^N \quad (9)$$

is nonzero.[12] For now, we shall neglect nonequilibrium effects and thus consider only those tunneling processes for which the initial state corresponds to the grain's ground state, i.e., $|i\rangle^N=|s_0,s_0\rangle^N$. In particular, we shall focus on two different types of equilibrium transitions: (A) transitions involving single-particle excitations whose resonance spacing, estimated from the electron density of states, is found to be much larger than observed in DGR's experiments and (B) transitions between different spin-wave states, of which only two transitions are found to have significant weight, leaving unexplained the large number of resonances seen in experiments.

A. Single-particle excitations

Apart from the multiplets $|s,m\rangle^N_0$ discussed in Sec. III B, higher-energy multiplets can be built by creating additional single-particle excitations, e.g., by starting from the bare multiplet constructed by applying the spin-lowering operator to the state $c^\dagger_{j'\uparrow}c_{j\uparrow}|s,s\rangle^N_0$, with $n_\downarrow<j\leq n_\uparrow$ and $j'>n_\uparrow$. However, their eigenenergies lie higher than those of the spin-wave multiplet $|s,m\rangle^N_0$ by an amount of order $\varepsilon_{j'}-\varepsilon_j$; this is at least of order of the single-electron level spacing, $d_{\rm maj}=4.61$ eV$/s_0$ (respectively, $d_{\rm min}=1.19$ eV$/s_0$), i.e., rather large compared to $d_{\rm obs}$ [cf. (P1)]; thus the mechanism causing the observed abundance of low-energy excitations, whatever it is, cannot only involve purely single-particle excitations, but must also involve spin excitations.

TABLE I. Matrix elements $M^{j\sigma}_{fi}$ and excitation energies ΔE^+_{fi} of those final states $|f\rangle^{N+1}=|s_f,m_f\rangle^{N+1}_0$ that can be reached from the initial state $|i\rangle^N=|s_0,s_0\rangle^N_0$ by adding a spin-σ electron to level $j_1=n_\uparrow+1$ or $j_2=n_\downarrow+1$.

$(j\sigma)$	s_f,m_f	$M^{j\sigma}_{fi}$	ΔE^+_{fi}
$(j_1\uparrow)$	$s_0+1/2,s_0+1/2$	1	$E_C+\varepsilon_{F,\rm maj}+d_{\rm maj}-(U/2)(s_0+3/4)-h/2$
$(j_1\downarrow)$	$s_0+1/2,s_0-1/2$	$1/\sqrt{2s_0+1}$	$E_C+\varepsilon_{F,\rm maj}+d_{\rm maj}-(U/2)(s_0+3/4)+h/2$
$(j_2\downarrow)$	$s_0-1/2,s_0-1/2$	1	$E_C+\varepsilon_{F,\rm min}+d_{\rm min}+(U/2)(s_0+1/4)+h/2$

B. Spin-wave excitations

We shall now study transitions between two multiplets of spin-wave states, with initial states $|i\rangle^N=|s_i,m_i\rangle^N$ and final states $|f\rangle^{N+1}=|s_f,m_f\rangle^{N+1}$. Consider first the large-field regime $h\gg h_{\rm sw}$ (where $h_{\rm sw}=g_{\rm eff}\mu_B\mu_0H_{\rm sw}$). Since here $\mathcal{H}_{\rm Zee}$ dominates over $\mathcal{H}_{\rm uni}$, we may set $k_N=0$ and construct the matrix elements $M^{j\sigma}_{fi}$ using the *bare* spin-wave multiplets $|s_i,m_i\rangle^N_0$ and $|s_f,m_f\rangle^{N+1}_0$. The condition $M^{j\sigma}_{fi}\neq 0$ then implies the *spin selection rules* $|s_f-s_i|=1/2$ and $|m_f-m_i|=1/2$.

Among all possible final states $|f\rangle$ satisfying these selection rules, Table I lists those three which can be reached by adding an electron to the *lowest available* levels of $|s_0,s_0\rangle^N_0$, namely, $j_1=n_\uparrow+1$ and $j_2=n_\downarrow+1$: A spin-$\uparrow$ electron can be added only to level j_1 (Table I, row 1), whereas a spin-$\downarrow$ electron can be added to either level j_1 (row 2) or j_2 (row 3).

The excitation energies ΔE^+_{fi} (Table I, column 4) of the $(j_1\uparrow)$ and $(j_1\downarrow)$ transitions are degenerate at $h=0$ and Zeeman split as a function of h, but, in accord with (P3), this splitting will not be observable: the weight of the $(j_1\downarrow)$ transition is smaller than that of the $(j_1\uparrow)$ transition (Table I, column 3) by a Clebsch-Gordan coefficient of order $1/(2s_0)$ which is negligibly small for large-s_0 grains.[1] The $(j_1\uparrow)$ and $(j_2\downarrow)$ transitions both have large, comparable weights, and would produce resonances with large-h slopes of opposite signs. Depending on whether the difference in their excitation energies (Table I, column 4) is close to or far from 0 (it is at most of order $d_{\rm maj}-U/2$, i.e., $\lesssim 3$ meV for a 4-nm-diameter Co particle[14]), either both or only one of the $(j_1\uparrow)$ and $(j_2\downarrow)$ transitions would be observable in the regime of lowest excitation energies (say, $\lesssim 0.5$ meV). However, in an equilibrium tunneling scenario, this leaves unexplained the large observed density of tunneling resonances (P1), since,

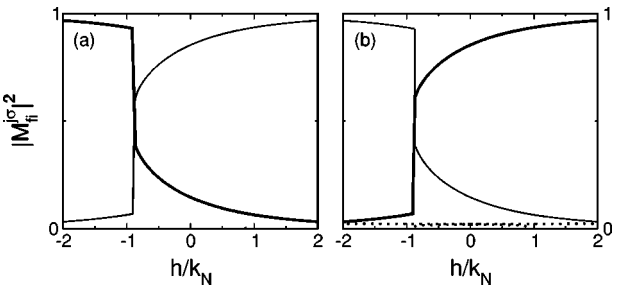

FIG. 2. Matrix elements $M_{fi}^{j\sigma}$ for the transitions $|s_i,s_i\rangle^N \rightarrow |s_f,m_f\rangle^{N+1}$ ($s_i=20$), calculated for $\mathcal{H}_{\rm uni}+\mathcal{H}_{\rm Zee}$ and plotted as functions of h/k_N sweeping positive to negative, for the following final states: (a) $|s_i-\frac{1}{2},s_i-\frac{1}{2}\rangle^{N+1}$; (b) $|s_i+\frac{1}{2},s_i+\frac{1}{2}\rangle^{N+1}$ (solid lines) and $|s_i+\frac{1}{2},s_i-\frac{1}{2}\rangle^{N+1}$ (dotted lines). Compared to these, all other final states have negligible matrix elements. The solid lines are thick for $M_{fi}^{j\uparrow}$ and thin for $M_{fi}^{j\downarrow}$ (both contribute to the *same* transition $|i\rangle \rightarrow |f\rangle$).

apart from these two transitions, there are no others with significant weight *and* excitation energies less than $d_{\rm min}$ ($d_{\rm maj}$).

Next we argue that this problem persists also for the case with anisotropy, where $k_N \neq 0$. *A priori* one might have expected to see more low-lying excitations then, since the selection rule $|m_f-m_i|=1/2$ no longer applies if the matrix elements $M_{fi}^{j\sigma}$ are formed using the exact spin-wave multiplets $|s_0,m_i\rangle^N$ and $|s_0\pm 1/2,m_f\rangle^{N+1}$, which are not S^z eigenstates. We have therefore numerically diagonalized $\mathcal{H}_{\rm Zee}+\mathcal{H}_{\rm uni}$,[18] as a function of h/k_N, for a few selected values of s_0, to determine the eigenstates $|s_0,m_i\rangle^N$ and $|s_0\pm 1/2,m_f\rangle^{N+1}$ and calculate the matrix elements $M_{fi}^{j\sigma}$ (Fig. 2), for both spin-increasing and -decreasing transitions ($s_f=s_0\pm 1/2$, $j=n_{\uparrow/\downarrow}+1$).

We find that in both cases, the transition probability $\Sigma_\sigma |M_{fi}^{j\sigma}|^2$ from $|s_0,s_0\rangle^N$ to $|s_0\pm 1/2,s_0\pm 1/2-n\rangle^{N+1}$ is very much larger for $n=0$ than for *any* other $n\neq 0$ state. This is the same trend as that found in Table I. Thus, even though $\mathcal{H}_{\rm uni}$ causes violations of one of the spin selection rules, the extra transitions have too little weight to explain the large density of low-energy excitations that is observed (P1).[19]

Apart from the fact that only two of the above-discussed transitions have significant weight there are two additional important considerations which lead us to conclude that the abundance of resonances seen in experiments cannot be explained by equilibrium spin-wave transitions alone: (i) First, the resonances associated with final states $|s_f,m_f\rangle$ that differ only in m_f would have a spacing of order k_N [≈ 0.01 meV], i.e., much smaller than the observed resonance spacing. (ii) Second, for high magnetic fields these resonances would exhibit a systematic increase in the magnitude of their slopes (which is $\propto |s_i-m_f|$) that was not observed in experiment. We therefore assert that the large density of resonances cannot be explained by equilibrium transitions alone; we will explore nonequilibrium effects below.

V. NONEQUILIBRIUM TRANSITIONS

Since the large density of resonances (P1) cannot be explained by equilibrium transitions [neither single-particle excitations (Sec. IV A) nor spin-wave excitations (Sec. IV B)], we shall in this section explore nonequilibrium effects. Our conclusion will be that a combination of nonequilibrium spin and single-particle excitations produces a much denser spectrum of tunneling states than expected within an independent-electron model. For a spin of $s_0 \simeq 1000$, this nonequilibrium scenario gives a resonance spacing of $\simeq 0.2$ meV for the spacing of resonances due to the tunneling of minority electrons, in accord with the observed resonance spacing.

Nonequilibrium spin accumulation had of course already been studied previously in the context of single-electron transistors with ferromagnetic components,[6,20] and spin accumulation for nanograins with discrete energy levels was first analyzed by Barnás *et al.*[21] However, these analyses all employed a single-particle description in which all states that were considered were simple Slater determinants of single-particle states. Within our present model, we have to go beyond this simple picture by considering the true many-body eigenstates of the Hamiltonian, which are in general *linear combinations* of Slater determinants.

After explaining the general idea of nonequilibrium processes in ferromagnetic grains in Sec. V A, we shall describe different nonequilibrium scenarios. For each, we calculate the corresponding theoretical tunnel spectra and compare resonance spacings and the number of resonances with DGR's measurements. We show in Sec. V B that nonequilibrium spin excitations lead to resonance spacings as observed in measurements and, in Sec. V C, that Zeeman splittings are suppressed for large spin s_0. A combination of spin and single-particle excitations (Sec. V D) significantly enhances the number of tunneling resonances achievable for a given setting of the gate voltage, making it possible to explain the large number of resonances observed by DGR even for the case of a small Coulomb-blockade threshold (i.e., weak nonequilibrium).

A. General master equation

In general, N-electron states other than the ground state can be populated during the process of current flow, and this may affect the experimental tunneling spectrum.[12,22] A simple scenario is illustrated in Fig. 3. Even if a first tunneling event causes a ''charging'' transition from the N-electron ground state $|\gamma_g\rangle^N$ to the $(N\pm 1)$-electron ground state $|\gamma_g\rangle^{N\pm 1}$, it may be energetically possible for the subsequent ''discharging'' tunneling transition to return the particle to an excited N-electron state $|\gamma_e\rangle^N$ instead of $|\gamma_g\rangle^N$, provided the applied voltage is sufficiently large, $eV \gtrsim E_e^N - E_g^N$. Likewise, further charging and discharging transitions may allow any of a large ensemble of states to be occupied at higher and higher levels of an energy ladder, terminating only when an energy-increasing transition requires more energy than the applied voltage provides. As the voltage is increased, the total current (or conductance) may increase stepwise (or show peaks) when thresholds are crossed to allow higher-energy transitions up the nonequilibrium ladder, thereby changing the occupation probabilities of the ensemble of nonequilibrium states and opening new tunneling channels.

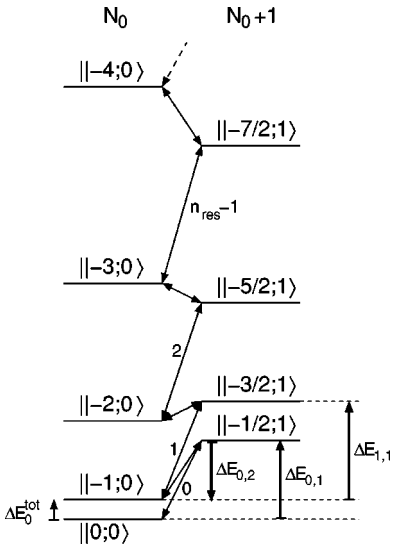

FIG. 3. Illustration of a nonequilibrium scenario involving only spin ground states, $||\delta s;\delta N\rangle \equiv |s_0+\delta s, s_0+\delta s\rangle^{N_0+\delta N}$, for the case in which the first electron that tunnels is a minority electron ($\alpha=-1$) that enters the grain ($p=+1$). Here δs and δN characterize the spin with respect to the overall spin ground state: $\delta s = s - s_0$ and $\delta N = N - N_0$ (see Secs. III C and V B). The vertical arrows indicate the energy differences $\Delta E^{\alpha p}_{n,1}$, $\Delta E^{\alpha p}_{n,2}$, and $\Delta E^{\rm tot}_0$. Charging transitions are numbered as $n=0,\ 1,\ 2\cdots$.

Let $\{\gamma\}$ be the set of all states involved in a nonequilibrium ladder of excitations, i.e., the set of all discrete states with a nonzero occupation probability $P(\gamma)$ for a given bias voltage, gate voltage, temperature, and magnetic field. To find the occupation probability $P(\gamma)$ for all the states $|\gamma\rangle$ of the ladder one has to solve a normalization condition $\Sigma_{\gamma'} P(\gamma') = 1$ and a stationary master equation of the form[12]

$$0 = \sum_{\gamma' \neq \gamma} \{\Sigma_{\gamma\gamma'} P(\gamma') - \Sigma_{\gamma'\gamma} P(\gamma) + \Sigma^{\rm el}_{\gamma\gamma'} P(\gamma') - \Sigma^{\rm el}_{\gamma'\gamma} P(\gamma) + \Sigma^{\rm sf}_{\gamma\gamma'} P(\gamma') - \Sigma^{\rm sf}_{\gamma'\gamma} P(\gamma)\}, \tag{10}$$

for each γ. The first (second) term in Eq. (10) describes the rate at which the probability of a given configuration increases (decreases) due to electrons tunneling onto or off the grain, and the remaining terms are associated with electronic relaxation and spin-flip relaxation on the grain, respectively.

$\Sigma_{\gamma\gamma'}$ is the total tunneling-induced transition rate from initial state $|\gamma'\rangle$ to final state $|\gamma\rangle$. Considering sequential tunneling only, it has the form

$$\Sigma_{\gamma\gamma'} = \sum_{r=L,R} \sum_{p=\pm} \Sigma^{rp}_{\gamma\gamma'}, \tag{11}$$

where $\Sigma^{r+}_{\gamma\gamma'}$ ($\Sigma^{r-}_{\gamma\gamma'}$) involves the coherent transfer of an electron onto (from) the grain from (onto) lead r and is given by

$$\Sigma^{r+}_{\gamma\gamma'} = \Gamma^r \sum_{i\sigma} |\langle\gamma|c^\dagger_{i\sigma}|\gamma'\rangle|^2 f(E_\gamma - E_{\gamma'} - e\overline{V}_r),$$

$$\Sigma^{r-}_{\gamma\gamma'} = \Gamma^r \sum_{i\sigma} |\langle\gamma|c_{i\sigma}|\gamma'\rangle|^2 f(E_\gamma - E_{\gamma'} + e\overline{V}_r).$$

Here $f(E) = 1/(e^{E/k_BT}+1)$ is the Fermi function and $e\overline{V}_r$ is the electrostatic potential-energy difference between lead r and the grain,

$$e\overline{V}_r \equiv eV_r - eV_D. \tag{12}$$

The third and fourth terms in Eq. (10) describe electronic (spin-conserving) relaxation processes inside the grain. For simplicity, we shall only consider electronic relaxation between energetically ''neighboring'' single-particle levels, i.e., we take

$$\Sigma^{\rm el}_{\gamma\gamma'} = \Gamma^{\rm el} \sum_{i\sigma} |\langle\gamma|c^\dagger_{(i-1)\sigma} c_{i\sigma}|\gamma'\rangle|^2. \tag{13}$$

(Generalizations of this assumption are straightforward, though cumbersome.) The last two terms of Eq. (10) describe the rate at which the probability of a given distribution increases (decreases) due to spin-flip relaxation in the ferromagnetic grain. For simplicity we shall assume all spin-flip relaxation rates to be much smaller than all other rates, $\Gamma^{\rm sf} < \Gamma^{r/l}, \Gamma^{\rm el}$, and hence take $\Sigma^{\rm sf}=0$ throughout this paper.[23] (Again, it is straightforward to consider generalizations of this case.) Moreover, all rates Γ are assumed to be independent of the specific single-particle level $i\sigma$ involved.

The current through the grain can then be calculated as[12]

$$I_r = e \sum_{\gamma\gamma'} (\Sigma^{r+}_{\gamma\gamma'} - \Sigma^{r-}_{\gamma\gamma'}) P(\gamma'). \tag{14}$$

B. Spin accumulation

In a ferromagnetic particle, in addition to the nonequilibrium occupation of single-electron states discussed previously for nonmagnetic particles,[22] nonequilibrium spin excitations are possible, too, if the spin-flip rate $\Gamma^{\rm sf}$ is smaller than the tunneling rate $\Gamma^{\rm tun}$.[23] In this case a ladder of transitions will occur between states with different total spin s, causing each to have a finite occupation probability and thus leading to *spin accumulation* on the grain.[6,20,21]

The simplest nontrivial case, namely, a ladder of spin multiplet ground states $|s,s\rangle$ (see Fig. 3) was already briefly discussed in Ref. 3. Below we shall discuss this case in more detail. We shall calculate the resonance spacing of steps in the current (or of peaks in the differential conductance) and the number of resonances for transitions between spin ground states. We shall characterize spin ground states by their *spin and charge relative to the overall ground state*, i.e., we shall write

$$||\delta s;\delta N\rangle \equiv |s_0+\delta s, s_0+\delta s\rangle^{N_0+\delta N}, \tag{15}$$

with δs and δN as defined in Sec. III C after Eq. (6). We shall find that the resonance spacing agrees very well with DGR's measurements.

Consider a sequence of nonequilibrium transitions forming a ''ladder'' ($L^{\alpha p}$) with ''rung index'' $n=0,1,2,\ldots,$

where each rung corresponds to a ''charging'' transition ($L^{\alpha p}_{n,1}$) followed by a ''discharging'' transition'' ($L^{\alpha p}_{n,2}$):

$$||\alpha p n;0\rangle \xrightarrow{L^{\alpha p}_{n,1}} ||\alpha p(n+1/2);p\rangle \xrightarrow{L^{\alpha p}_{n,2}} ||\alpha p(n+1);0\rangle.$$

(Above, the notation $||\delta s;\delta N\rangle$ is used.) The indices p and α are used to distinguish whether the *first* electron that tunnels enters or leaves the grain, $p=(+1,-1)$, and whether it is a majority or minority electron, $\alpha=(\mathrm{maj},\mathrm{min})=(+1,-1)$.

Using Eq. (7), the threshold energy costs for transitions $L^{\alpha p}_{n,1}$ and $L^{\alpha p}_{n,2}$ can be calculated to be[24]

$$\Delta E^{\alpha p}_{n,1}=E[\alpha p(n+1/2);p]-E(\alpha p n;0)$$
$$=\Delta E^{\alpha p}_{0,1}+n[d_\alpha-U/2], \tag{16a}$$

$$\Delta E^{\alpha p}_{n,2}=E[\alpha p(n+1);0]-E[\alpha p(n+1/2);p]$$
$$=\Delta E^{\alpha p}_{0,2}+n[d_{\bar\alpha}-U/2], \tag{16b}$$

with

$$\Delta E^{\alpha p}_{0,1}=d_\alpha(1+p)/2+E_C+p(\bar\varepsilon_F+\alpha d_0/2)-U/8,$$

$$\Delta E^{\alpha p}_{0,2}=d_{\bar\alpha}(1-p)/2-E_C-p(\bar\varepsilon_F-\alpha d_0/2)-3U/8.$$

(Above, the notation $\bar\alpha$ means $\overline{\mathrm{maj}=\mathrm{min}}$ and $\overline{\mathrm{min}=\mathrm{maj}}$.) Note that the total-energy cost for the combined transitions $L^{\alpha p}_{0,1}$ and $L^{\alpha p}_{0,2}$, namely,

$$\Delta E^{\alpha p}_{0,\mathrm{tot}}\equiv\Delta E^{\alpha p}_{0,1}+\Delta E^{\alpha p}_{0,2}=d_\alpha\frac{1+p}{2}+d_{\bar\alpha}\frac{1-p}{2}+p\alpha d_0-\frac{U}{2}, \tag{17}$$

is always $\geqslant 0$; this follows intuitively from the fact that $\Delta E^{\alpha p}_{0,\mathrm{tot}}$ is the excitation energy between the overall ground state $||\delta s;\delta N\rangle=||0;0\rangle$ and the adjacent-spin ground state $||\alpha p;0\rangle$, and more formally from condition (8) on d_0.

Assuming that the peaks in the conductance are due to successive charging transitions becoming accessible as the bias voltage is increased, the resonance spacing for the ladder $L^{\alpha p}$ can readily be calculated using Eqs. (16):

$$\delta E^{\alpha p}_{\mathrm{res}}\equiv\Delta E^{\alpha p}_{n+1,1}-\Delta E^{\alpha p}_{n,1}=d_\alpha-U/2. \tag{18}$$

This result, which evidently depends only on whether the charging transition involves the tunneling of a majority or minority electron, $\alpha=(\mathrm{maj},\mathrm{min})$, can be intuitively understood as follows: The resonance spacing, $\delta E^{\alpha p}_{\mathrm{res}}$, is a difference of energy differences, i.e., a type of (discrete) second derivative of the total energy. The contribution d_α reflects the discrete second derivative with respect to the quasiparticle number of the energy involved in creating n-particle-like or hole-like excitations relative to the overall ground state, using only α electrons. The term $-U/2$ reflects the discrete second derivative with respect to the spin of the exchange energy. The partial cancellation between d_α and $-U/2$ in Eq. (18) reflects the opposite signs of the kinetic and exchange energies in the Hamiltonian (2), and is thus very generic. Very significantly, since $U/2$ and d_{min} (but not d_{maj}) happen to be almost equal, this partial cancellation of two rather large energies produces a much smaller energy,

$$\delta E^{\mathrm{maj},p}_{\mathrm{res}}\simeq(4.6-1.0)\ \ \mathrm{eV}/s_0=3.6\ \ \mathrm{eV}/s_0, \tag{19a}$$

$$\delta E^{\mathrm{min},p}_{\mathrm{res}}\simeq(1.2-1.0)\ \ \mathrm{eV}/s_0=0.2\ \ \mathrm{eV}/s_0, \tag{19b}$$

where we used the parameter estimates given in Secs. II and III.[25] This brings us to one of the main conclusions of this paper: *the small resonance spacing of* 0.2 meV *observed by DGR is consistent with prediction* (19b) *for minority-electron charging events* if the ground state spin is assumed to be about $s_0\simeq 1000$, which is within the estimated size range of DGR's grains. Satisfactorily, the conclusion that minority electrons dominate the charging transitions, which was reached independently by Canali and MacDonald too,[11] has recently been confirmed experimentally for DRG's gated device, as has been the conclusion that nonequilibrium physics is involved [cf. points (P4) and (P5) of Sec. II].

We shall therefore henceforth consider only the case in which charging transitions are due to minority electrons, i.e., we take $\alpha=\mathrm{min}$ (but for notational brevity will sometimes still use the index α instead of ''min''). The conductance will then show a limited number, say, $n^{\mathrm{ch}}_{\mathrm{res}}$, of resonances due to *charging* transitions, with a rather small spacing of $d_{\mathrm{min}}-U/2$, followed by an unlimited number of resonances due to *discharging* transitions, with a much larger spacing of $d_{\mathrm{maj}}-U/2$. This can be seen as follows: let us consider for definiteness a circuit with $V_L=-V_R=V/2$, and suppose that $eV>0$, so that electrons flow from left to right through the ferromagnetic grain. Then transition $L^{\alpha p}_{n,1}$ involves tunneling across the left junction if $p=1$, or the right junction if $p=-1$ [and likewise $L^{\alpha p}_{n,2}$ involves tunneling across junction (R,L) for $\bar p=(-1,1)$]. The voltage thresholds, say, $eV^{\alpha p}_{n,1}$ (or $eV^{\alpha p}_{n,2}$), needed to overcome the energy cost $\Delta E^{\alpha p}_{n,1}$ (or $\Delta E^{\alpha p}_{n,2}$) in order for the charging transition $L^{\alpha p}_{n,1}$ (or the discharging transition $L^{\alpha p}_{n,2}$) to occur, are determined by the conditions

$$pe\bar V_p\geqslant\Delta E^{\alpha p}_{n,1}, \tag{20a}$$

$$\bar p e\bar V_{\bar p}\geqslant\Delta E^{\alpha p}_{n,2}. \tag{20b}$$

Here $e\bar V_p$, the electrostatic potential-energy difference between lead p and the grain, is [from Eq. (12)] related to the actual applied voltage by

$$e\bar V_p=peVB_p-e\tilde V_g, \tag{21}$$

where $B_p\equiv(C_{\bar p}+C_g/2)/C$ is a capacitance ratio which converts applied voltage to energy,[12] and $e\tilde V_g\equiv e(Q_0+V_gC_g)/C$ is an offset energy. It follows from Eqs. (20) and (21) that $V^{\alpha p}_{n,1}$ and $V^{\alpha p}_{n,2}$ are given by

$$B_p eV^{\alpha p}_{n,1}=\Delta E^{\alpha p}_{n,1}+pe\tilde V_g, \tag{22a}$$

$$B_{\bar p}eV^{\alpha p}_{n,2}=\Delta E^{\alpha p}_{n,2}-pe\tilde V_g. \tag{22b}$$

In particular, the threshold voltage $V_{0,1}^{\alpha p}$ for the first charging transition, $L_{0,1}^{\alpha p}$, determines the measured size of the Coulomb-blockade region (in energy units), say, E_C^{thresh}:

$$E_C^{\text{thresh}} \equiv eV_{0,1}^{\alpha p} B_p = \Delta E_{0,1}^{\alpha p} + pe\tilde{V}_g . \tag{23}$$

This enables us to eliminate $pe\tilde{V}_g$ from Eq. (22) and write it as [using Eqs. (16) and (17)]

$$B_p eV_{n,1}^{\alpha p} = n(d_\alpha - U/2) + E_C^{\text{thresh}}, \tag{24a}$$

$$B_{\bar{p}} eV_{n,2}^{\alpha p} = n(d_{\bar{\alpha}} - U/2) - E_C^{\text{thresh}} + \Delta E_{0,\text{tot}}^{\alpha,p}. \tag{24b}$$

Now, whenever $E_C^{\text{thresh}} \gtrsim \frac{1}{2}\Delta E_{0,\text{tot}}^{\alpha,p}$, i.e., whenever E_C^{thresh} is not too small, the inequality

$$eV_{n,1}^{\alpha p} > eV_{n,2}^{\alpha p} \tag{25}$$

will hold for sufficiently small values of n (at least for $n=0$). However, for large enough n it will cease to hold, since for the case $\alpha = \min$ that we are considering, the "step size" $d_{\text{maj}} - U/2$ for $eV_{n,2}^{\alpha p}$ is much larger than the "step size" $d_{\min} - U/2$ for $eV_{n,1}^{\alpha p}$. Thus, the first few measured conductance resonances will be due to a sequence of (rather closely spaced) *charging* transitions, as opposed to (much more widely spaced) discharging transitions, because each time the bias voltage is incremented by $eV_{n,1}^{\alpha p}$ to make the next charging transition $L_{n,1}^{\alpha p}$ energetically accessible, this bias voltage increment is already large enough (namely, $> eV_{n,2}^{\alpha p}$) to also allow the discharging transition $L_{n,2}^{\alpha p}$ to occur. However, once the inequality Eq. (25) is violated, the subsequent discharging transition $L_{n,2}^{\alpha p}$ will become possible only after the total bias voltage increment reaches $eV_{n,2}^{\alpha p}$, i.e., henceforth *discharging* (instead of charging) transitions will determine the conductance resonances, which will henceforth be spaced much more widely.

To calculate the total number of closely spaced resonances due to charging transitions, $n_{\text{res}}^{\text{ch}}$, we must thus determine how large n can become before the condition Eq. (25) ceases to hold. Using Eqs. (24) and $B_p + B_{\bar{p}} = 1$, this condition can be rearranged to yield an expression for $n_{\text{res}}^{\text{ch}}$, which is found to be given by the smallest integer larger than or equal to

$$1 + \frac{E_C^{\text{thresh}} - B_p \Delta E_{0,\text{tot}}^{\min,p}}{B_p(d_{\text{maj}} - U/2) - B_{\bar{p}}(d_{\min} - U/2)}. \tag{26}$$

The prediction that $n_{\text{res}}^{\text{ch}}$ increases linearly with E_C^{thresh} is in qualitative agreement with Fig. 2 of Ref. 1.[3] However, it is not quite consistent with more recent data on Co grains,[2] where, even when the Coulomb-blockade threshold was very small ($E_C^{\text{thresh}} \lesssim 1$ meV), the differential conductance showed many (>10) peaks, i.e., many more than Eq. (26) would predict. To illustrate this, we have solved Eq. (10) numerically for the discussed transitions and calculated the current for the parameters of the model and a threshold charging energy of $E_C^{\text{thresh}} = 0.8\ \text{eV}/s_0$ as a function of eVB_L [see Fig. 4(a)]. The calculated current shows three steps in the plotted region. Experimental data (see Fig. 1 in Ref. 2) on the other hand show ≈ 12 resonances for the parameters used.

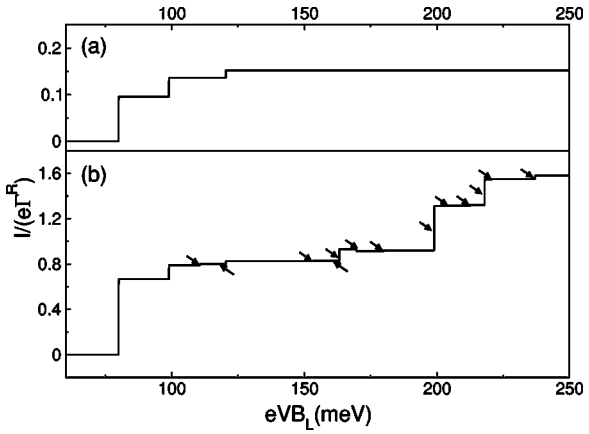

FIG. 4. Current as a function of eVB_L for the following parameters: $\alpha = \min$, $p = +1$, $s_0 = 10$, $d_{\min} = 1.19\ \text{eV}/s_0$, $d_{\text{maj}} = 4.61\ \text{eV}/s_0$, $U = 2\ \text{eV}/s_0$, $B_L = 0.3$, $B_R = 0.7$, $E_C^{\text{thresh}} = 0.8\ \text{eV}/s_0$, $E_{0,\text{tot}}^{\alpha p} = 0\ \text{eV}/s_0$, $\Gamma^L/\Gamma^R = 0.8$, $\Gamma^{\text{sf}} = 0$, and $T = 80$ mK (Ref. 26). (a) Only spin excitations. (b) Spin excitations and single-particle excitations: $\Gamma^{\text{el}}/\Gamma^R = 10^6$. Arrows mark additional current steps due to combined spin and single-particle excitations. No significance should be attached to step heights here, since they depend on (unknown) tunneling matrix elements, which for simplicity we took to be all equal (Ref. 27). Parameters are chosen according to Fig. 1 of Ref. 2.

To summarize the conclusions of this section, a nonequilibrium scenario involving only spin ground states, and assuming charging transitions involving minority electrons, results in a spacing of resonances, $\delta E_{\text{res}} \approx 0.2$ meV for $s_0 = 1000$, which agrees roughly with the spacing observed. However, the number of resonances predicted by Eq. (26) is sometimes much smaller than observed, i.e., when E_C^{thresh} is small (on the order of $d_{\min}$).

C. Spin-wave excitation

In the preceding section, we considered only transitions between different spin ground states, $|s,s\rangle$. In the present section we summarize what happens when this scenario is extended to include *all* higher-lying states of the corresponding multiplets $|s,m\rangle$ (see Fig. 5). We find that this results in a fine structure for the current steps, which would, however, be resolvable only for *very* low temperatures[28] and hence would not be expected to be observable in DGR's present measurements. Moreover, we find that the Zeeman splitting of resonances is strongly suppressed for a large spin $s_0 \gg 1$. A more detailed discussion of the results presented here will be given in the Appendix.

Figure 5 shows a typical set of possible transitions between a series of spin multiplets $|s,m\rangle$, with s values $\cdots s_0 + 1$, $s_0 + 1/2$, s_0, $s_0 - 1/2$, $s_0 - 1 \cdots$. The anisotropy energy lifts the degeneracy of the $2s+1$ spin-wave states in each multiplet, producing a typical level spacing of order k_N. Figure 6 shows the current for transitions between different spin-wave states as illustrated in Fig. 5. Figure 6(a) (zero

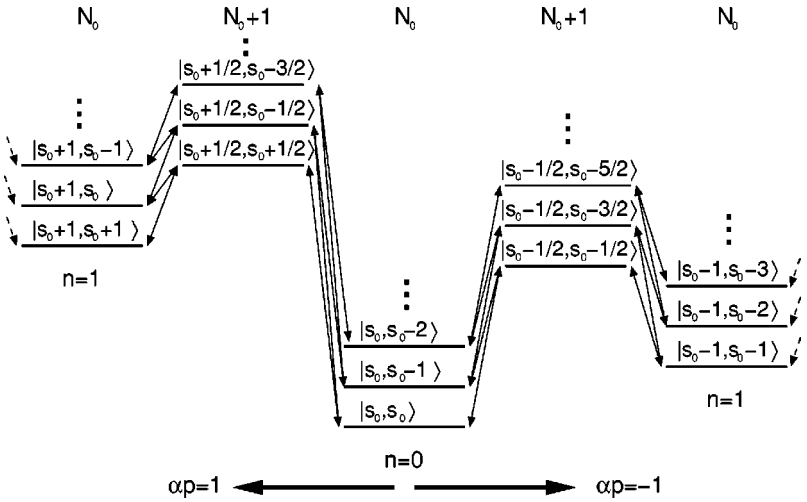

FIG. 5. Illustration of a nonequilibrium scenario involving spin-wave states: Different multiplets $|s,m\rangle$ for N_0 and N_0+1 electrons on the grain are depicted. Due to selection rules only specific transitions (marked by arrows) are possible.

magnetic field) and Fig. 6(d) (nonzero magnetic field) show that the current features a series of large-scale steps, similar to those discussed previously with a spacing that can be shown to still be given by $d_{\min}-U/2(=0.2\ \mathrm{eV}/s_0)$. In a magnetic field each of these steps splits in two substeps, as illustrated into Fig. 6(e), which depicts one of these large-scale steps in more detail. Furthermore, if the temperature is sufficiently low, additional fine structure emerges in the form of a set of very fine ministeps [Fig. 6(c) and Fig. 6(f)]; these can be associated with transitions between the various spin wave states of neighboring multiplets. The spacing between these ministeps, which is $k_N/s_0(\approx 0.01\ \mathrm{meV}/s_0)$, is due to the lifting of the degeneracy within each multiplet due to the anisotropy energy. The two substeps in Fig. 6(e) can be interpreted as follows: they arise due to Zeeman splitting between the group of all S^z-decreasing transitions [ministeps on the right side in Fig. 6(f)] and the group of all S^z-increasing transitions [ministeps on the left side in Fig. 6(f)]. Note that the S^z-decreasing step in Fig. 6(e) is significantly higher than the S^z-increasing step, implying that S_z-decreasing transitions carry considerably more weight than S_z-increasing ones. Moreover, the difference in their weights increases substantially as s_0 is increased, as can be seen from Fig. 7, which shows how the difference in step heights for S_z-decreasing and -increasing transitions evolves with s_0.

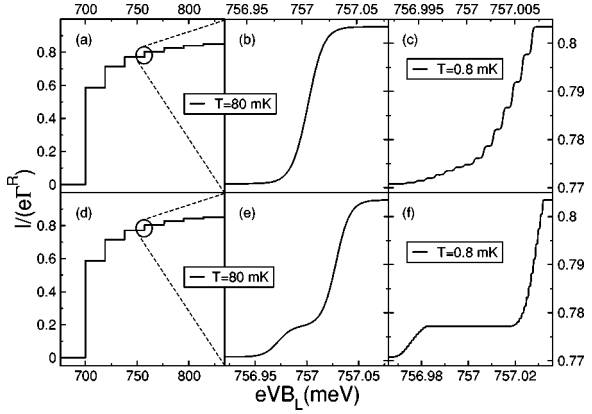

FIG. 6. Current as a function of eVB_L for the following parameters: $\alpha=\min$, $p=+1$, $s_0=10$, $d_{\min}=1.19\ \mathrm{eV}/s_0$, $d_{\mathrm{maj}}=4.61\ \mathrm{eV}/s_0$, $U=2\ \mathrm{eV}/S_0$, $B_L=0.4$, $B_R=0.6$, $k_N=0.01$ meV, $\Gamma^L/\Gamma^R=0.8$, $\Gamma^{\mathrm{sf}}=0$, and $\Gamma^{\mathrm{el}}=0$, and a Coulomb-blockade region of 7 eV/s_0; (a)–(c) $h=0$ meV; (d)–(f) $h=0.05$ meV; (b) and (e) show the fourth current step of (a) and (d) for $T=80$ mK; (c) and (f) show the same step for a lower temperature of $T=0.8$ mK. No significance should be attached to step heights here, since they depend on (unknown) tunneling matrix elements.

Let us now summarize the consequences of the nonequilibrium scenario discussed above for the tunneling spectra measured by DGR. (i) First, the temperature in DGR's experiments, namely, $T\approx 80$ mK, is too high for the fine current steps of Figs. 6(c) and 6(f), due to spin-wave excitations, to have been observable. Instead, only the large-scale current steps of Figs. 6(a) and 6(d) would be observable. The observed resonance spacing of $\delta E_{\mathrm{res}}\approx 0.2$ meV [cf. (P1)] indeed does agree with that expected for minority-electron charging transitions and $s_0\approx 1000$ [cf. Eq. (19b)]. (ii) Second, the nonequilibrium scenario discussed above can also account for the fact (P3) that the vast majority of the observed transitions within a given sample shift in energy with

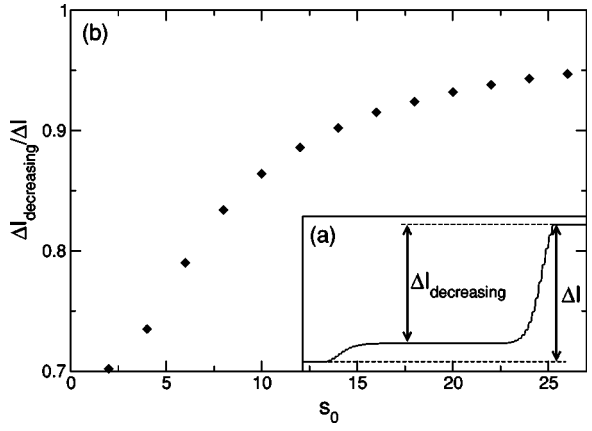

FIG. 7. (a) A Zeeman-split current step, where ΔI_{decr} is the overall height of steps due to all S^z-decreasing transitions and $\Delta I=\Delta I_{\mathrm{decr}}+\Delta I_{\mathrm{incr}}$ is the overall current step. (b) $\Delta I_{\mathrm{decr}}/\Delta I$, calculated numerically for various s_0 values for the second step in the current and $\Gamma^L/\Gamma^R=0.1$.

a similar slope for large magnetic fields, since for $s_0 \gg 1$, S^z-decreasing transitions carry far more weight than S^z-increasing transitions (Fig. 7).

The reader interested in the details of the results presented in this subsection is encouraged to read the Appendix. In particular, there it is explained that the reason for the difference in weights between S_z-decreasing and S_z-increasing transitions can be traced to Clebsch-Gordan coefficients in the tunneling matrix elements.

D. Spin and single-particle excitations

We saw in Secs. V B (and V C) that a nonequilibrium scenario involving transitions between different spin states (spin-wave states) of the grain leads to resonances in tunneling spectra spaced by $d_{\min} - U/2$, which for $s_0 = 1000$ gives a value of ≈ 0.2 meV, as observed in experiments. However, these scenarios are not always able to explain the large number of resonances observed, since $n_{\rm res}^{\rm ch}$ given in Eq. (26) depends strongly on the threshold charging energy and can become as small as *two* when $E_C^{\rm thresh}$ is of order of or smaller than $d_{\min}$.

We shall now argue below that the abundance of resonances measured by DGR can be explained by taking the analysis one step further, namely, by including single-particle excitations in addition to spin excitations. For the spin excitations we shall henceforth restrict our considerations to transitions between spin ground states as in Sec V B, since we saw in Sec. V C that DGR's experimental temperature was too high to resolve the fine structure due to spin-wave transitions. Furthermore, we shall assume[23] $\Gamma^{\rm el} \gg \Gamma^{\rm tun}$, and hence shall take into account only excited single-particle states involving a *single* particle-hole pair, i.e., states which can be reached from the corresponding ground states by a *single* tunneling transition, namely, a majority/minority electron entering the N-electron grain or a majority/minority electron leaving the $N+1$-electron grain.[27] Figure 8 illustrates some examples.

We solved Eq. (10) numerically for the parameters of Fig. 1 in Ref. 2 and calculated the current; the result is shown in Fig. 4(b). The current shows 16 steps in the plotted region. Note that the calculation of the current was done for the same parameters as in Fig. 4(a) where only spin excitations were taken into account. The arrows in Fig. 4(b) mark all additional resonances with respect to 4(a) which arise due to a combination of spin and single-particle excitations. Most of the resonances in Fig. 4(b) are due to tunneling of minority electrons, namely, 14 resonances out of 16. This results from the very different density of states of minority and majority electrons at the Fermi energy [cf. (P4)].

Thus, when single-particle excitations are considered in addition to nonequilibrium spin accumulation, additional resonances appear at higher voltages, so that the number of resonances increases significantly. The resonances are no longer equally spaced, as was the case for pure spin excitations, but the average spacing is of the same order of magnitude.

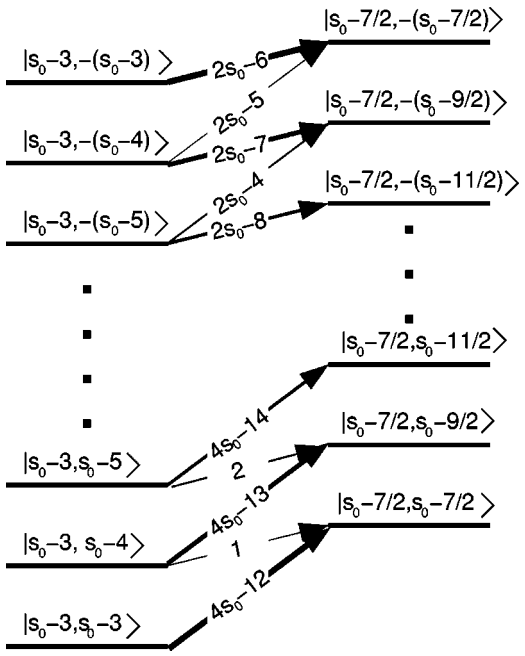

FIG. 8. Transitions from the (s_0-3) to the $(s_0-7/2)$ multiplet. Arrows indicate all transitions allowed by the selection rule that S^z can change only by $\pm 1/2$. The width of an arrow schematically indicates the size of the Clebsch-Gordan coefficient involved in the matrix element of the corresponding transition. The energy separations between the various levels are not drawn to scale. The order in which transitions become possible as the applied voltage is increased is given by the numbers in the arrows, which range from 1 to $2s_0-6$ for S^z-increasing transitions, and then from $2s_0-5$ to $4s_0-12$ for S^z-decreasing transitions.

We also investigated the gate-voltage dependence of these resonances. Figure 9 shows resonances as a function of bias voltage (eVB_L) and threshold charging energy $E_C^{\rm thresh}$.

Note that $E_C^{\rm thresh}$ depends linearly on gate voltage via Eq. (23). Figure 9 should be compared with the experimental plot in Ref. 2 [Fig. 3(a)], which shows the conductance as a function of gate and bias voltages. There a number of tun-

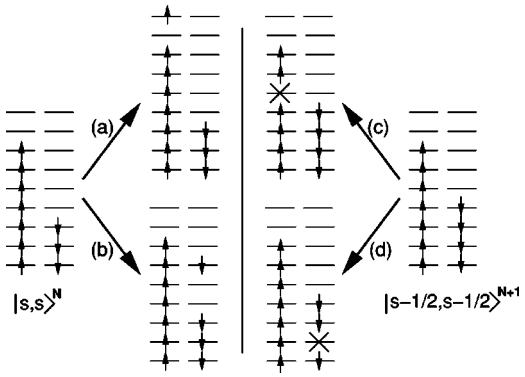

FIG. 9. Illustration of single-particle excitations: Examples of excited single-particle states, which can be reached from the ground state $|s,s\rangle^N$ by (a) a majority electron or (b) a minority electron entering the grain, or from a $|s-1/2,s-1/2\rangle^{N+1}$ state by (c) a majority electron or (d) a minority electron leaving the grain.

neling resonances disappears as the Coulomb threshold is reduced [cf. (P5)]. The same qualitative trend can be found in Fig. 9. In particular, both plots agree in that *not all* resonances disappear for a small Coulomb threshold. However a more detailed understanding of the observed gate-voltage dependence of resonances, i.e., which specific resonance disappears at which voltage, would require a more systematic examination, and a more reliable microscopic model.

VI. CONCLUSIONS

In summary, we have shown that nonequilibrium spin and single-particle excitations within our model are able to explain most of the experimental data by DGR on tunneling spectroscopy of ultrasmall ferromagnetic grains. In particular, we showed that the small resonance spacing of 0.2 meV observed by DGR [cf. (P1)], and their observation that resonances correspond predominately to tunneling of minority electrons [cf. (P4)], are both consistent with prediction (19b) in Sec. V B. We argued that a fine structure of resonances due to spin-wave excitations would not be observable in DGR's experiment due to a too high temperature (see Sec. V C). This is in agreement with the experimentally observed resonance spacing [cf. (P1)]. The nonequilibrium scenario discussed above can also account for the fact (P3) that the vast majority of the observed transitions within a given sample shift in energy with a similar slope for large magnetic fields: We argued that the observed resonances are indeed *not* expected to show Zeeman splitting in an applied magnetic field, because the spin-decreasing transitions carry significantly more weight than spin-increasing ones, due to Clebsch-Gordan coefficients in the tunneling matrix elements (Sec. V C and the Appendix). We showed that a combination of nonequilibrium spin and single-particle excitations can account for the number of resonances observed in DGR's experiment with a level spacing of order of 0.2 meV as observed [cf. (P1), Sec. V D]. Finally, we found that within our model the number of resonances increases with increasing gate voltage, which is in qualitative agreement with experimental data by DGR [compare Fig. 9 with Fig. 3(a) of Ref. 2].

Last, we want to mention that in our phenomenological model spin-orbit interaction was incorporated only in an indirect way, in that it gave rise to the anisotropy term in the Hamiltonian [Eq. 2]. In a microscopic theory spin-orbit coupling would couple quasiparticle and spin excitations, so that the separate and independent treatment of them used in our analysis would not be possible to the same extent as was above. Including the effects of such a coupling is beyond the scope of the present paper, but is a very interesting subject for future work.

ACKNOWLEDGMENTS

We thank C. Canali and A. MacDonald for advance communication of their work and several very helpful discussions, and J. Becker, D. Boese, A. Brataas, E. Chudnovsky, A. Garg, C. Henley, D. Loss, W. Mörke, A. Pasupathy, J. Petta, and G. Schön for fruitful discussions. We give special thanks to D.C. Ralph, M. Deshmukh, E. Bonet, and S. Guéron for a fruitful collaboration in which they not only made their data available to us but also significantly contributed to the development of the theory. This work was supported by the DFG through SFB195, the DFG Program ''Semiconductor and Metallic Clusters,'' and by the DAAD-NSF.

APPENDIX: DETAILS ON NONEQUILIBRIUM SPIN-WAVE EXCITATIONS

In this Appendix we discuss the results of Sec. V C on nonequilibrium spin-wave excitations in more detail. Figure 5 illustrates the possible transitions between different spin-wave states of ''neighboring'' multiplets. For simplicity, we assume that both the magnetic field and the easy axis lie in the z direction, so that the selection rule $|m_f - m_i| = 1/2$ holds.

We solved Eq. (10) numerically for a spin[26] of $s_0 = 10$ and a Coulomb-blockade region of 7 eV/s_0 (as in Fig. 2, sample 3 of Ref. 1), and calculated the current for zero magnetic field [Figs. 6(a)–6(c)], and nonzero applied field [Figs. 6(d)–6(f)]. Figure 6(a) shows the current as function of energy ($B_L eV$) for a temperature of $T = 80$ mK and zero magnetic field, $h = 0$ eV. The current displays seven equally spaced steps. These steps belong to transitions between successive sets of pairs of multiplets, e.g., the first one belongs to transitions between $|s_0, m\rangle$ and $|s_0 - 1/2, m'\rangle$, the next one to transitions between $|s_0 - 1, m\rangle$ and $|s_0 - 3/2, m'\rangle$, etc. Figure 6(b) shows the fourth current step of Fig. 6(a) on a finer energy scale. In Fig. 6(c) the same step is shown for a lower temperature of $T = 0.8$ mK, at which it now reveals substructure in the form of 14 finer steps. These *small* steps correspond to transitions between various states of the two multiplets, $|s_0 - 3, m\rangle$ and $|s_0 - 7/2, m\rangle$, namely, the first *small* step in Fig. 6(c) corresponds to a transition, $|s_0 - 3, \pm(s_0 - 4)\rangle \rightarrow |s_0 - 7/2, \pm(s_0 - 7/2)\rangle$, the next one to $|s_0 - 3, \pm(s_0 - 5)\rangle \rightarrow |s_0 - 7/2, \pm(s_0 - 9/2)\rangle$, etc. The last step in Fig. 6(c) corresponds to $|s_0 - 3, \pm(s_0 - 3)\rangle \rightarrow |s_0 - 7/2, \pm(s_0 - 7/2)\rangle$. It can be checked easily, using Eq. (2f), that their spacing is given by $k_N / s_0 (\simeq 0.01$ meV/$s_0)$. Similarly, all other steps of Fig. 6(a) (except for the first one) have a substructure of smaller steps belonging to all transitions between neighboring multiplets that are allowed by the selection rules (as indicated in Fig. 5). Note that the number of (large-scale) steps in Fig. 6(a) is still given by Eq. (26) of Sec. V B, with a spacing given by $d_{\min} - U/2 (= 0.2$ eV/$s_0)$.

In Figs. 6(d)–6(f) a similar set of plots is shown as in Figs. 6(a)–6(c), but now in the presence of an applied magnetic field, $h = 0.05$ meV. Figure 6(d) shows the current itself. Figures 6(e) and 6(f) again show the fourth current step for two different temperatures. Figure 6(e) shows that the step of Fig. 6(b) has Zeeman split into two steps and Fig. 6(f) shows that these two steps correspond to two groups of transitions, namely, all S^z-*increasing* transitions (steps on the left side) and S^z-*decreasing* transitions (right side) between the two multiplets $|s_0 - 3, m\rangle$ and $|s_0 - 7/2, m\rangle$. The fact that Fig. 6(f) shows many more steps than Fig. 6(c) results from the fact that the applied magnetic field lifts the degeneracy of

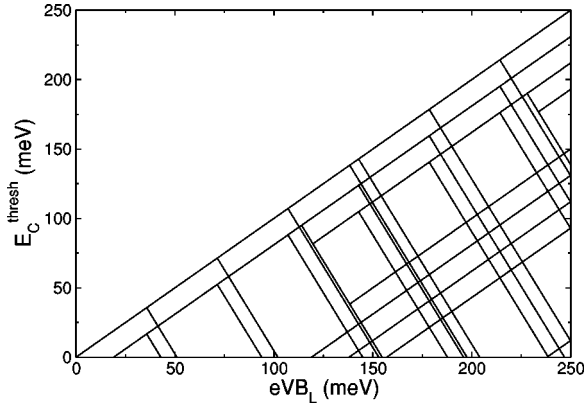

FIG. 10. Resonances as a function of E_C^{thresh} and eVB_L for the same parameters as in Fig. 4. As E_C^{thresh} is increased additional resonances appear. Note that Fig. 4(b) corresponds to a cut through Fig. 9 for fixed E_C^{thresh} (gate voltage).-

states $|s,\pm m\rangle$. The first step in Fig. 6(f) belongs to a transition $|s_0-3,s_0-4\rangle\rightarrow|s_0-7/2,s_0-7/2\rangle$, the next one to $|s_0-3,s_0-5\rangle\rightarrow|s_0-7/2,s_0-9/2\rangle$, etc. The last step corresponds to $|s_0-3,s_0-3\rangle\rightarrow|s_0-7/2,s_0-7/2\rangle$.

Since the individual substeps in Fig. 6(f) are higher for the S^z-decreasing transitions (to the right of the plot) than for the S^z-increasing transitions (to the left), the second large-scale step in Fig. 6(e) is higher than the first. The reason for this height difference lies in the fact that matrix elements for transitions between different spin-wave states contain Clebsch-Gordan coefficients: Let us consider the two multiplets which give rise to the current steps in Fig. 6(f), namely, the (s_0-3) and the $(s_0-7/2)$ multiplet. The energy levels of these multiplets are schematically depicted in Fig. 10. The first transition between the multiplets which becomes possible as the applied voltage is increased is a S^z-increasing transition, namely, the $|s_0-3,s_0-4\rangle\rightarrow|s_0-7/2,s_0-7/2\rangle$ transition at the bottom of the ladder. As the voltage is increased further, more and more S^z-increasing transitions become possible. (In Fig. 10 they are numbered $1,2,\ldots,2s_0-6$.) The last S^z-increasing transition, namely, $|s_0-3,-(s_0-3)\rangle\rightarrow|s_0-7/2,-(s_0-7/2)\rangle$, lies at the top of the ladder. As we increase the applied voltage further the first S^z-decreasing transition $[|s_0-3,-(s_0-4)\rangle\rightarrow|s_0-7/2,-(s_0-7/2)\rangle]$ becomes possible (at the top of the ladder). As we increase the voltage further, more and more S^z-decreasing transitions become possible, the last transition $(|s_0-3,s_0-3\rangle\rightarrow|s_0-7/2,s_0-7/2\rangle)$ lying at the bottom of the ladder. Let us now compare Clebsch-Gordan coefficients involved in the different transitions. In Fig. 10 their magnitude is schematically indicated by the width of the arrows marking the transitions. For example, the Clebsch-Gordan coefficient involved in the matrix element for the first S^z-increasing transition $(|s_0-3,s_0-4\rangle\rightarrow|s_0-7/2,s_0-7/2\rangle)$ as well as the first S^z-decreasing transition $[|s_0-3,-(s_0-4)\rangle\rightarrow|s_0-7/2,-(s_0-7/2)\rangle]$ in Fig. 6(f) (and Fig. 10) is of order $O(1/s)$, hence these transitions carry very little weight. By increasing the applied voltage, so that more transitions become accessible, the Clebsch-Gordan coefficients for S^z-increasing transitions increase from $O(1/s)$ to $O(1)$ as we go *up* the ladder and those for S^z-decreasing transitions likewise increase from $O(1/s)$ to $O(1)$ as we subsequently go *down* the ladder. Now, the occupation probabilities P, in general, are larger[29] for lower-lying spin-wave states than for higher-lying ones. Since transitions out of these more strongly populated lower-lying states of the spin-(s_0-3) multiplet have a Clebsch-Gordan coefficient of order $O(1)$ if they are S^z decreasing, and of order $O(1/s)$ if they are S^z increasing, we conclude that the total weight of all S^z-decreasing transitions is larger than that of all S^z-increasing transitions. The net result is that the S^z-decreasing step in Fig. 6(e) is higher than the S^z-increasing step.

The relative heights of the two large-scale steps in Fig. 6(e) are analyzed in Fig. 7, or more precisely, the height of the current step due to all S^z-decreasing transitions, ΔI_{decr}, relative to the total height of the current step ΔI. Figure 7 confirms that *S^z -decreasing transitions typically carry significantly more weight than S^z -increasing transitions*. Moreover, with increasing spin s_0 the height of ΔI_{decr} increases strongly relative to ΔI, so that for large s_0 no Zeeman splitting is expected.

*Email address: kleff@theorie.physik.uni-muenchen.de

[1] S. Guéron, M.M. Deshmukh, E.B. Myers, and D.C. Ralph, Phys. Rev. Lett. **83**, 4148 (1999).

[2] M.M. Deshmukh, S. Kleff, S. Guéron, E. Bonet, A.N. Pasupathy, J. von Delft, and D.C. Ralph, Phys. Rev. Lett. **87**, 226801 (2001).

[3] S. Kleff, J. von Delft, M. Deshmukh, and D.C. Ralph, Phys. Rev. B **64**, 220401 (2001).

[4] D.C. Ralph, C.T. Black, and M. Tinkham, Phys. Rev. Lett. **74**, 3241 (1995); **76**, 688 (1996); **78**, 4087 (1997).

[5] K. Ono, H. Shimada, and Y. Ootuka, J. Phys. Soc. Jpn. **66**, 261 (1997); **67**, 2852 (1998).

[6] J. Barnaś and A. Fert, Europhys. Lett. **44**, 85 (1998).

[7] J. Barnaś and A. Fert, Phys. Rev. Lett. **80**, 1058 (1998).

[8] Note also that spin-dependent transport through quantum dots with weak exchange coupling has been considered by D. Weinmann, W. Häusler, W. Pfaff, B. Kramer, and U. Weiss, Phys. Rev. Lett. **26**, 467 (1994); and also by Y. Tanaka and H. Akera, Phys. Rev. B **53**, 3901 (1996).

[9] K.E. Johnson, J. Appl. Phys. **87**, 5365 (2000).

[10] S. Sun, C.B. Murray, D. Weller, L. Folks, and A. Moser, Science **287**, 1989 (2000).

[11] C.M. Canali and A.H. MacDonald, Phys. Rev. Lett. **85**, 5623 (2000).

[12] Jan von Delft and D.C. Ralph, Phys. Rep. **345**, 61 (2001).

[13] D. Davidović and M. Tinkham, Phys. Rev. Lett. **83**, 1644 (1999).

[14] D. A. Papaconstantopoulos, *Handbook of the Band Structure of Elemental Solids* (Plenum, New York, 1986).

[15] We use $d_\sigma=1/[N_a\mathcal{N}_\sigma(\varepsilon_F)]$, where $\mathcal{N}_\sigma(\varepsilon)$ is the spin-dependent bulk density of states per atom (Ref. 14). Using bulk values is appropriate for nanoscale grains, since quantum chemical calculations (Ref. 30) on Ni clusters have shown that $\mathcal{N}_\sigma(\varepsilon)$ has

converged to its bulk shape already for N_a as small as 6. For Co, Ref. 14 gives $\mathcal{N}_\uparrow(\varepsilon_F)=0.18\ \mathrm{eV}^{-1}$, $\mathcal{N}_\downarrow(\varepsilon_F)=0.7\ \mathrm{eV}^{-1}$.

[16] A model similar in spirit was introduced independently by Canali and MacDonald (Ref. 11).

[17] A more general form for the anisotropy of an ultrasmall ferromagnetic grain would be $\mathcal{H}_{\mathrm{anis}}=-\Sigma_{ab}\Sigma_{ij}S_i^a\mathcal{K}_{ij}^{ab}S_j^b$ where $\mathcal{K}_{ij}^{aa}$ is a Hermitian, traceless tensor ($\Sigma_a\mathcal{K}_{ij}^{aa}=0$), which describes the energy cost for rotating the various spins $\vec{S}_j$ (see Ref. 3).

[18] S. Kleff, Diploma thesis, Universität Karlsruhe, 2000.

[19] This is in agreement with Fig. 2 of Ref. 11.

[20] A. Brataas, Yu.V. Nazarov, J. Inoue, and G.E.W. Bauer, Eur. Phys. J. B **9**, 421 (1999).

[21] Previous predictions of spin accumulation always involved ferromagnetic leads; see, e.g., J. Barnaś, J. Martinek, G. Michalek, B.R. Bulka, and A. Fert, Phys. Rev. B **62**, 12 363 (2000), and references therein.

[22] O. Agam, N.S. Wingreen, B.L. Altshuler, D.C. Ralph, and M. Tinkham, Phys. Rev. Lett. **78**, 1956 (1997).

[23] For DGR's Co nanograins of Ref. 1 or Ref. 2, we estimate Γ^{tun} from the conductance to be $\Gamma^{\mathrm{tun}}\approx Gd_{\mathrm{min}}/e^2\approx 10^9\ \mathrm{s}^{-1}$ or $10^7\ \mathrm{s}^{-1}$, respectively. By comparison, we estimate the rate for spin-conserving electronic relaxation to be $\Gamma^{\mathrm{el}}\approx 10^9\ \mathrm{s}^{-1}$, if we use Eq. (8) of Ref. 22 (though it is not entirely clear that that formula, derived for ordinary metals, is also applicable to a strongly correlated ferromagnetic system such as Co). Thus, for the grains of Ref. 1 or Ref. 2, Γ^{el} is of the same order or larger than Γ^{tun}. As for the spin-flip rate Γ^{sf}, we do not know of a reliable way to estimate it from theoretical considerations, except to state that it is expected to be much smaller than the nonspin-flip relaxation rate, $\Gamma^{\mathrm{sf}}\ll\Gamma^{\mathrm{el}}$. The condition for the occurrence of nonequilibrium spin accumulation, namely, $\Gamma^{\mathrm{tun}}>\Gamma^{\mathrm{sf}}$, would thus readily be satisfied for Ref. 1, but for Ref. 2, one would need Γ^{sf} to be more than two orders-of-magnitude smaller than our estimate for Γ^{el}. This difference is rather large, but might also indicate that our estimate for Γ^{el} is unreliably large.

[24] We do not consider $\mathcal{H}_{\mathrm{uni}}$ or $\mathcal{H}_{\mathrm{Zee}}$ here, since in DGR's experiments the relevant energy scales, $k_N\approx 0.01$ meV and $h_{\mathrm{max}}\approx 0.5$ meV, are much smaller than the exchange splitting of majority and minority bands, $\Delta_F\approx 2$ eV in Co.

[25] For general values of d_{min}, d_{maj}, and U, one of the resonance spacings in $d_\alpha-U/2$ in Eq. (18) could become negative. However, only positive resonance spacings lead to observable conductance resonances. Thus, if $d_{\mathrm{min}}-U/2<0$ (or $d_{\mathrm{maj}}-U/2<0$), only transitions involving the tunneling of majority (or minority) electrons would lead to observable conductance resonances. Note, though, that the stability condition Eq. (8) precludes both energy differences from being negative at the same time.

[26] The ground-state spin of $s_0=10$ chosen here is of course unrealistically small, but for larger values the numerical analysis becomes intractably complicated. We do believe, though, that the conclusions drawn from our numerical analysis are generic.

[27] For simplicity we have not included excited single-particle states which can only be reached from ground states by multiple (nonequilibrium) excitations. However, these transitions certainly exist as $\Gamma^{\mathrm{el}}\approx\Gamma^{\mathrm{tun}}$ (see Ref. 23). Since in our simple model, we assumed a constant level spacing for spin-up and for spin-down electrons, [see Eq. (2)] these additional transitions would lead to resonances at precisely the same energies as the ones that we do discuss. In a more realistic model with nonuniform level spacing, however, we would expect that such additional transitions lead to clusters of resonances. Depending on the strength of the fluctuations in level spacing and the amount of nonequilibrium, such clusters would or would not be resolvable in experiments such as DGR's. We have not analyzed these complications in detail, however, since our aim is merely to show that even by including only *part* of the single-particle excitations possible, the number of resonances is increasing significantly [with respect to $n_{\mathrm{res}}^{\mathrm{ch}}$ given by Eq. (26)], making it possible to explain the large number of resonances in DGR's measurements.

[28] For a spin of $s_0=1000$ this fine structure would only be resolvable for $T<0.2$ mK. This follows from a comparison of the spacing of the fine structure steps, k_N/s_0, with k_BT.

[29] Though this statement is of course somewhat of an oversimplification, since the occupation probabilities depend in a sensitive way on the transition matrix elements, we do believe that it is, ultimately, the reason why in our numerical calculations (Fig. 7) the total weight of S^z-decreasing transitions turns out to be larger than for S^z-increasing transitions. Note also, that in the calculation for Fig. 6 no relaxation processes were taken into account, which of course is not realistic. In particular, in the presence of relaxation it is to be expected that states with negative S^z eigenvalues, which, loosely speaking correspond to a spin vector pointing in a direction opposite to the applied magnetic field, would have little or no occupation probability. However, we believe that our qualitative discussion of the role of Clebsch-Gordan coefficients above would still be valid for nonzero relaxation since a nonzero relaxation would simply lead to an even larger occupation probability for the low-lying spin-wave states and smaller occupation probability for the high-lying states. Therefore, we expect the inclusion of nonzero relaxation to make the ratio $\Delta I_{\mathrm{decr}}/\Delta I$ even larger and the width of the plateau between the S^z-increasing and S^z-decreasing steps in Fig. 6(e) wider.

[30] G. Pacchioni and N. Rösch, Acc. Chem. Res. **28**, 390 (1995), and references therein.